PHYSICAL REVIEW B VOLUME 7, NUMBER 5 1 MARCH 1973

Interference Effects in a Superconducting Aluminum Film; Vortex Structure and Interactions

A. T. Fiory
Bell Laboratories, Murray Hill, New Jersey 07974
(Received 28 July 1972)

Interference transitions are observed in the mixed state of a granular oxygen-doped superconducting aluminum film when vortex-lattice motion is driven by applying superimposed rf and dc electric currents. An analysis of the properties of the transitions in the small-signal rf resistivity is made according to a recent theory of vortex motion in an inhomogeneous superconductor by Schmid. The theory satisfactorily explains the effect, which is due to the dissipative excitation of vortex-lattice fluctuations. New information on vortex structure and interactions at low magnetic field is obtained. The vortex-lattice shear-constant measurements agree with the theoretical work of Fetter, Hohenberg, and Pincus and of Brandt. A pinning-potential correlation function also comes out of the measurements and its component factors are identified: the structural-defect correlation function and the vortex-free-energy distribution. The maximum in the free-energy density at the vortex axis, which is larger than Ginzburg-Landau-theory predictions, suggests the presence of the core excitations discussed in a recent microscopic theory of vortex structure.

I. INTRODUCTION

In a previous paper, which reported finding quantum interference transitions in the electrical resistivity of an aluminum-film sample, an analogy was drawn between such vortex-lattice-flow effects and Josephson-effect phenomena.[1] Remaining unexplained, however, were (i) why the vortex lattice should choose a preferred orientation relative to the direction of flow and (ii) which mechanism is responsible for coupling rf and dc applied currents.

The experimental results stimulated theoretical work by Schmid, who formulated a phenomenological model for vortex motion within the random pinning potential of an inhomogeneous superconductor.[2] Schmid has shown that dynamic excitation of long-wavelength deformations of the vortex lattice results in an additional anisotropic dissipation, favoring a certain orientation of the lattice. Related experimental observations of current-induced lattice orientation have recently been reported. Alignment of the Bragg planes in niobium is influenced by a transport current, according to recent neutron-diffraction work by Simon and Thorel.[3] In an atomic-beam experiment, Brown and King observed magnetic field periodicities just outside a vanadium foil in the mixed state.[4] Success in that experiment depends upon having a preferred orientation of the vortex lattice, which was apparently achieved when a transport current was applied.

The theory also explains the steplike structure observed in our plots of rf voltage and dc current versus dc electric field. Analogies between observations of flux-flow voltages in the mixed state and the Josephson effect, familiar in weakly coupled bulk superconductors, have been drawn in a number of theoretical papers, some having suggested possible experiments to demonstrate an analog to the ac Josephson effect.[5-7] It has been pointed out, however, that the coupling of external rf currents to the locally varying current oscillations associated with uniform flow of an extended vortex lattice is negligibly small, the lattice parameter being so much smaller than the electromagnetic wavelength.[8] The Anderson–Dayem bridge structure serves as an example of the limiting case where transverse vortex flow can exhibit an ac Josephson effect.[9] This geometry permits only a small number of vortices to be present in the bridge, with edge effects allowing an external rf current to synchronize the regular passage of vortex quanta. For the experiment under consideration in this paper, a novel manifestation of an analog to the ac Josephson effect takes place within a large superconducting sample through the intermediary interaction between vortices and random pinning forces. A significant aspect of these experiments, in distinction from the Anderson–Dayem experiment, is that coherent motion of the vortices is already present in the dc motion of the lattice and that the small rf current which is applied serves more as a probe than as a synchronizer of regular vortex motion.

We explore the ramifications of Schmid's theoretical results by making a detailed study of the transition steps in the rf resistivity of an oxygen-doped aluminum film. From measured widths of the transitions, we compute experimental values of the vortex-lattice shear modulus c_{66}. At low magnetic fields and at temperatures not too close to T_c, these results compare favorably well with heretofore untested calculations for bulk systems

by Fetter, Hohenberg, and Pincus[10] and by Brandt.[11] Earlier results by Matricon are apparently in error by a factor of 6.[12] An upper bound to c_{66} in pure niobium was reported by Meincke and Reed who searched for a compressional vortex-lattice standing mode.[13]

From the sizes of the transition steps we infer the Fourier transform of the pinning-potential correlation function to give the correlation function for structural defects in the film and the free-energy-density distribution about a vortex at low magnetic field. In the latter result, we find that the free-energy density in the vortex core is significantly larger than that calculated from Ginzburg-Landau theory.[14] This suggests a qualitative experimental corroboration of recent microscopic calculations treating core states in pure superconductors.[15]

II. THEORY

Several years ago, Yamafuji and Irie introduced a model to explain the critical pinning current. Departing from previous pinning-force concepts, they showed that deformation of the vortex lattice accompanying flux flow plays an essential role, finding that the pinning current is proportional to the square of the local pinning forces divided by an elastic constant of the vortex lattice.[16] Webb and co-workers have extended the lattice deformation concepts in their studies of flux pinning.[17] Recently, Larkin and Ovchinnikov, in a further refinement, showed that the critical current is related to correlation functions of the structural inhomogeneities in the superconductor.[18] Using a phenomenological equation of motion containing viscous damping and lattice, random pinning, and Lorentz forces, Schmid has recently formulated a more detailed theory of the influence of pinning upon vortex motion.[2] The principal results he obtained are discussed at length below.

A. Interference Transitions

For a Lorentz force which is a sum of collinear rf and dc components, Schmid finds the following second-order correction to the flow velocity:

$$\langle \vec{V}_2 \rangle = \frac{-i}{\eta} \sum_{\vec{g}} \sum_{\vec{q}} \vec{k}(\vec{e}_q \cdot \vec{k}) \langle |u(\vec{k})|^2 \rangle \times \sum_{n'm'} (-1)^{n'+m'} J_{n'}\left(\frac{a\vec{e}_v \cdot \vec{k}}{\omega}\right) J_{m'}\left(\frac{a\vec{e}_v \cdot \vec{k}}{\omega}\right) \times \frac{e^{-i\omega(n'-m')t}}{K_t q^2 + i\eta(v\vec{e}_v \cdot \vec{k} - n'\omega)} . \quad (1)$$

We have jumped ahead to his conclusion that the shear deformations of small wave vector $\vec{q}$ predominate. Definitions of the terms are as follows: η is the phenomenological viscosity coefficient, $\vec{g}$ is the reciprocal-lattice vector, $\vec{k} = \vec{g} + \vec{q}$, $\vec{e}_q$ is the polarization of vortex-lattice deformation, $\langle |u(\vec{k})|^2 \rangle$ is the Fourier transform of the pinning-potential correlation function, $J_{n'}$ is the Bessel function of order n', ω is the angular frequency of the rf component of the applied current, a is the amplitude of zeroth-order rf velocity, v is the mean dc flow velocity, $\vec{e}_v$ is the unit vector parallel to the mean flow direction, $K_t = \varphi_0 c_{66}/B$, and c_{66} is the vortex-lattice shear constant. $\langle \vec{V}_2 \rangle$, which is proportional to the pinning current, exhibits a change in magnitude at the transition points, wherein an integral multiple of the rf frequency equals a frequency associated with the driven motion of the periodic vortex structure. Upon increasing v through one of these interference transitions, the rf component of $\langle \vec{V}_2 \rangle$ increases while the dc component decreases. We review in the following discussion three regimes for the rf current amplitude: $a = 0$, $a \sim v$, and $a \ll v$.

(i) For $a = 0$, Eq. (1) leads to an expression for the dc pinning current density,

$$J_p = \frac{c}{8BK_t} \sum_{\vec{g}} |\vec{e}_v \cdot \vec{g}| \, |\vec{g}|^2 \langle |u(\vec{g})|^2 \rangle . \quad (2)$$

It will be subsequently shown that $\langle |u(\vec{g})|^2 \rangle$ is a rapidly decreasing function of $|\vec{g}|$, so that J_p is anisotropic with respect to the orientation of the vortex lattice relative to $\vec{e}_v$. Hence, a specific orientation is taken by the moving vortex lattice, that which results in minimum entropy production, and corresponds to the relation

$$|\vec{e}_v \cdot \vec{g}| = \tfrac{1}{2}\sqrt{3}\, n g_1 , \quad (3)$$

where n is an integer and g_1 is a primitive reciprocal-lattice vector length. Theories of flux-flow resistance which neglect pinning find isotropic dissipation, in lowest order, and no preferred orientation.

(ii) For $a \sim v$, the dc current exhibits transition steps when the mean flow velocity satisfies the relation

$$v|\vec{e}_v \cdot \vec{g}| = n'\omega , \quad (4)$$

where n' is an integer, or equivalently, when the dc electric field takes on the following values:

$$E_{nn'} = \frac{2}{\sqrt{3}} \frac{Bn'\omega}{cng_1} = \frac{n'}{n} \frac{\omega}{2\pi c} \left(\frac{2\varphi_0 B}{\sqrt{3}}\right)^{1/2} . \quad (5)$$

Schmid has worked out a formula for the detailed shape of these steps, which are broadened by the excitation of vortex-lattice deformations. We do not pursue this result, as the formula for the dc current transtitions which Schmid obtains is a complicated double sum over Bessel-function amplitudes. The procedure required to unfold this sum to get the components of $\langle |u(\vec{g})|^2 \rangle$ is not as straightforward as it is in the low rf current re-

gime, discussed next.

(iii) For $a \ll v$, the dc current and field are not affected to lowest order in a, whereas the rf electric field is linear in the rf current. The in-phase component of the rf resistivity, ρ', computed from Eq. (1), shows transition steps when the dc electric field E_{dc} equals E_{n1}. (The 90° out-of-phase component contains peaks at $E_{dc} = E_{n1}$.) The shape of the transition steps in ρ' is given by

$$\rho' - \rho'_{n1} = \frac{3}{32\pi} \frac{\varphi_0^2 n^2 g_1^4}{\eta^2 c^2 K_t \omega} \sum_{m=-\infty}^{\infty} w_{nm}^2 \langle |u(w_{nm} g_1)|^2 \rangle \times \left(\arctan(\gamma n^3 x) - \frac{w_{nm}^2 - \frac{3}{2}n^2}{2w_{nm}^2} (\gamma n^3 x) \ln[1 + (\gamma n^3 x)^{-2}] \right), \tag{6}$$

where ρ'_{n1} are values of the resistivity when the dc electric field E_{dc} equals E_{n1}. Other symbols in Eq. (6) are

$$w_{nm}^2 = n^2 + nm + m^2, \qquad \gamma = 2\sqrt{3}\, g_1 K_t B/\eta c E_{11},$$

$$x = (E_{dc} - E_{n1})/E_{11}.$$

A logarithmic divergence is not observed experimentally, and presumably it is smeared out. Denoting the magnitude of the nth transition in ρ' by $\Delta\rho'_n$, it follows from Eq. (6) that

$$\Delta\rho'_n = \frac{3}{32} \frac{\varphi_0^2 n^2 g_1^4}{\eta^2 c^2 K_t \omega} \sum_m w_{nm}^2 \langle |u(w_{nm} g_1)|^2 \rangle. \tag{7}$$

A width to the nth transition, defined as the interval in x, centered about $x = 0$, corresponding to $\frac{1}{2}\Delta\rho'_n$, is denoted by δx_n. It is given by the solution of the following equation:

$$\arctan z_n = y_n z_n \ln(1 + z_n^{-2}) = \tfrac{1}{2}\pi, \tag{8}$$

where

$$z_n = \tfrac{1}{2}\gamma n^3 \delta x_n \tag{9}$$

and

$$y_n = \sum_m (w_{nm}^2 - \tfrac{3}{2}n^2) \langle |u(w_{nm} g_1)|^2 \rangle / 2 \sum_m w_{nm}^2 \langle |u(w_{nm} g_1)|^2 \rangle. \tag{10}$$

The terms of the sums in Eqs. (6), (7), and (10) correspond to certain rows of reciprocal-lattice points that obey Eq. (3). Results for regime (3) are applied in Secs. IV and V in order to determine $\langle |u(\vec{g})|^2 \rangle$ and c_{66} from measurements of $\Delta\rho'_n$ and δx_1.

B. Shear Modulus

Several calculations of c_{66} at low magnetic field $B \ll H_{c2}$ in bulk superconductors have been published. These will be compared to the experiment, owing to the lack of thin-film calculations for c_{66}. All of the results can be written

$$c_{66} = \frac{\alpha B H_{c2}}{4\pi\kappa^2}, \quad B \ll H_{c2}, \tag{11}$$

where the numerical coefficients obtained are $\alpha = 0.118$ by Brandt,[11] $\alpha = 0.125$ by Fetter, Hohenberg, and Pincus,[10] and $\alpha = 0.70$ by Matricon.[12] At high magnetic field, a calculation by Labusch finds[19]

$$c_{66} = \frac{0.48\kappa^2(2\kappa^2 - 1)H_c^2}{4\pi[1 + (2\kappa^2 - 1)\beta]^2} \left(1 - \frac{B}{H_{c2}}\right)^2. \tag{12}$$

C. Pinning Potential

The nature of the pinning-potential correlation function has been discussed by Larkin and Ovchinnikov for random fluctuations in mean free path l, electron-phonon coupling constant (equivalent to fluctuations in T_c), and thickness of the film t.[18] We are taking a simplified approach, and presume that the fractional fluctuation in the local-free-energy density within a vortex line can be written in the form

$$S(\vec{r}) = \frac{\delta F(\vec{r})}{\langle F(\vec{r}) \rangle} = \frac{\partial \ln\langle F(\vec{r}) \rangle}{\partial \ln l} \frac{\delta l}{l} + \frac{\partial \ln\langle F(\vec{r}) \rangle}{\partial \ln T_c} \frac{\delta T_c}{T_c} + \frac{\partial \ln\langle F(\vec{r}) \rangle}{\partial \ln t} \frac{\delta t}{t}. \tag{13}$$

$\langle\,\rangle$ denotes an ensemble average and $S(\vec{r})$ is a random function of position $\vec{r}$, as are $\delta l/l$, $\delta T_c/T_c$, and $\delta t/t$, characterizing the structural inhomogeneities in the film. The change in the self-energy of one vortex from the average over the ensemble equals the pinning potential, given by the convolution

$$U(\vec{r}) = \int d\vec{r}'\, F(\vec{r}') S(\vec{r}' + \vec{r}). \tag{14}$$

For a lattice of vortices, we define the Fourier transform of $U(\vec{r})$ as an integral over the hexagonal lattice cell [of area $A = 2/(\sqrt{3})g_1^2$],

$$u(\vec{g}) = (1/A) \int_{\text{cell}} d^2\gamma\, e^{-i\vec{g}\cdot\vec{r}} U(\vec{r}). \tag{15}$$

Similarly, we expand the following in a Fourier series:

$$F(\vec{r}) = \sum_{\vec{g}} f(\vec{g})\, e^{i\vec{g}\cdot\vec{r}}, \tag{16}$$

$$S(\vec{r}) = \sum_{\vec{g}} s(\vec{g})\, e^{i\vec{g}\cdot\vec{r}}, \tag{17}$$

with the result

$$u(\vec{g}) = A f(-\vec{g}) s(\vec{g}). \tag{18}$$

An expression for the Fourier-transformed pinning-potential correlation function follows from Eq. (18):

$$\langle |u(\vec{g})|^2 \rangle = |A f(\vec{g})|^2 \langle |s(\vec{g})|^2 \rangle. \tag{19}$$

Although the details of the various contributions to the function $S(\vec{r})$ are unknown for our aluminum film, it seems reasonable to consider a model in which the mean size of the structural inhomogeneities, denoted by d, is much smaller than either

vortex dimensions or the vortex-lattice constant. For such a model the correlation function $\langle S(\vec{R})S(0)\rangle$ is expected to be largest when $|\vec{R}|/d \lesssim 1$, and should equal $\sigma d/|\vec{R}|$ for $|\vec{R}|/d \gg 1$, where σ is the mean value $\langle |S(R)|^2\rangle$ and is a second constant of the model. The Fourier transform is therefore

$$|\vec{g}|^2\langle |s(\vec{g})|^2\rangle = (1/A)\int_{\text{cell}} d^2R\, e^{-i\vec{g}\cdot\vec{R}}[-\nabla^2\langle S(\vec{R})S(0)\rangle]$$

$$\approx (1/A)\oint -\nabla\langle S(\vec{R})S(0)\rangle\cdot\vec{n}\, dL \approx 0.5 g_1^3 \sigma d. \qquad (20)$$

Here, Green's theorem was applied with the approximation $e^{-i\vec{g}\cdot\vec{R}} \sim 1$ over the range where the integrand is large. $\vec{n}$ is a unit vector normal to the path in the line integral. The quantity σd, an equivalent constant for this model, is obtained from experimental data, as discussed in Sec. IV.

III. EXPERIMENTAL PROCEDURE

An oxygen-doped aluminum film, 1000 Å thick, was prepared by evaporating pure aluminum at a rate of 2 Å/sec in an oxygen atmosphere at a pressure of 6×10^{-5} Torr. The substrate, a Corning 7059 glass slide, was fire polished immediately before placing it into the vacuum chamber where it was located 13 cm away from the filament. A photoetched mask was used to produce the specimen whose shape is depicted in Fig. 1. Detailed parameters of this specimen are listed in Table I. H_{c2} was obtained from plots of resistivity versus magnetic field, and T_c is extrapolated from a plot of H_{c2} vs T. The BCS coherence distance ξ_0 was estimated by multiplying the pure-aluminum value of 16 000 Å by the ratio of the critical temperature of pure aluminum to that of the film. Estimates of the mean free path l, and the Ginzburg–Landau parameter κ were then obtained from the H_{c2} measurement.

Abeles had found that a similarly prepared sample has a granular structure whose mean grain size is 180 Å.[20] Data shown in the figures of this paper were taken on one film, although several other aluminum films were prepared with various resistivities and dimensions, and the data for those films are qualitatively the same.

Although the actual current distribution in our film is expected to be nonuniform near the edges, it is not considered in our analysis of the data. Several cylindrical films were made to demonstrate that edge effects are not necessary in order to observe interference transitions. A glass tube supporting the cylindrical film was fitted over a solid cylindrical iron magnet pole piece, and surrounded by a second hollow cylindrical iron pole piece. A small, specially shaped, permanent magnet established a fixed "radial" magnetic field in an annular cylindrical gap which, over the area of the film, was perpendicular to its surface. With current applied in the axial direction, one of the pole pieces serving as a return current path, the vortices move in a circular path about the circumference of the film, never having to be created or destroyed at edges. The interference effect was also observed in such films.

TABLE I. Parameters of the oxygen-doped aluminum film used in this work.

Thickness	1000 Å
l	40 Å
ξ_0	12 000 Å
T_c	1.6 K
Normal resistivity	9 $\mu\Omega$ cm
$\kappa(T_c)$	3.0
$\frac{-dH_{c2}}{dT}$	$\frac{610\ \text{Oe}}{\text{K}}$

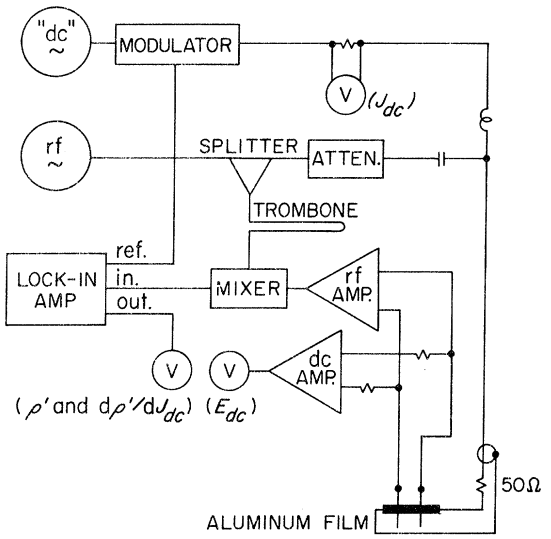

FIG. 1. Schematic diagram of experimental apparatus and aluminum film. The region between the specimen voltage probes is measured as 1.27×2.54 mm. The quantities measured are shown labeling the voltmeter symbols which represent inputs to an x–y recorder. All wires are 50-Ω coax.

Data were taken with the specimen immersed in pumped liquid helium over the temperature range $1.14 < T < 1.56$ K. Mixed rf, ac, and dc currents were applied through a single 50-Ω coaxial cable, terminated with a 50-Ω metal glaze resistor wired in series with the specimen, as shown in Fig. 1. rf currents ranged in frequency from 50 to 150 MHz. ac modulation was at 250 Hz and the dc was swept in 1 min. Two additional coaxial leads connected two voltage probes on the sample to both dc and rf differential amplifiers. The rf amplifier consisted of a matched balun transformer in front of an unbalanced rf amplifier. Measurements of the flux-flow rf voltage V_{rf} were made by

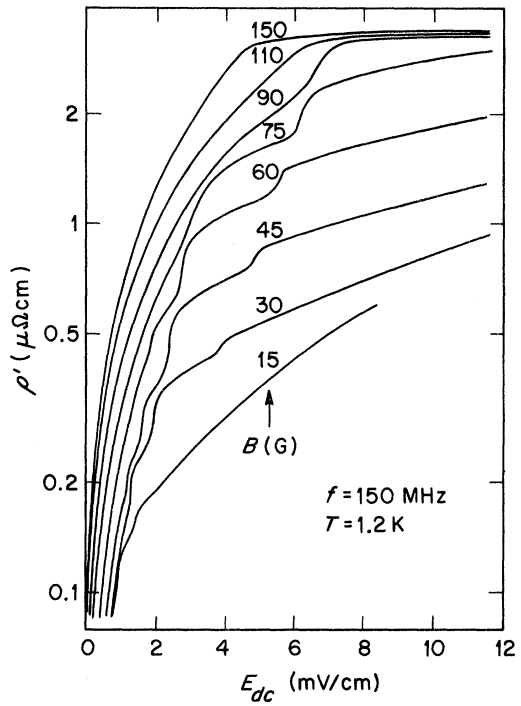

FIG. 2. rf resistivity (on log scale) vs dc electric field for various values of the magnetic field.

chopping the dc current at 250 Hz and synchronously detecting the mixer output. The derivative of the rf voltage with respect to dc current was obtained by superimposing a small 250-Hz modulation upon the dc current sweep. A steady background signal from reactive pickup is blocked by these procedures. The chopping technique takes advantage of the fact that the rf voltage for zero dc current is negligible compared to its value when there is dc flux flow.

Recorder tracings of both the rf voltage and the signal proportional to its derivative with respect to the dc current were made for various values of the applied magnetic field and of the temperature. A representative sample of these data are shown in Fig. 2, where a conversion to rf resistivity ρ', and dc electric field E_{dc}, was made. ρ' is independent of the magnitude of the rf current as long as it is small compared to the dc current. An rf amplitude on the order of 10% of the dc current was used. Plots of the out-of-phase component of the rf voltage (not shown) display peaks at those values of E_{dc} where the in-phase component shows steps. In Fig. 3, a typical derivative signal is plotted.

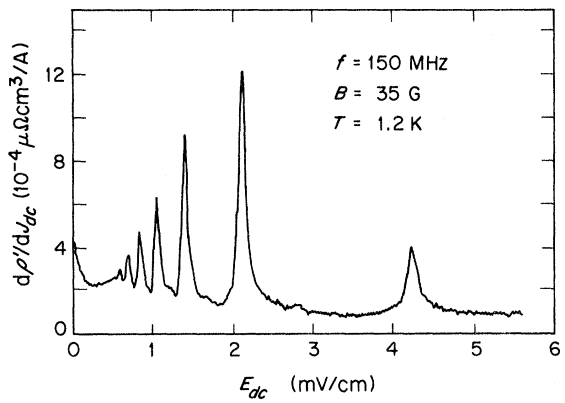

FIG. 3. Derivative of the rf resistivity with respect to dc current vs dc electric field.

IV. PROFILE OF $\langle|u(\vec{g})|^2\rangle$ AND VORTEX STRUCTURE

As the first application of the Schmid theory, we analyze the size of the transitions in the rf resistivity curves, examples of which are in Fig. 2. Steps in ρ' appear at certain values of the dc field, E_{n1}, which are proportional to n^{-1}, where n is an integer. The height of the nth step, denoted by $\Delta\rho'_{n1}$, is measured by extrapolating the asymptote of each rounded tail of the step to $E_{dc} = E_{n1}$ and taking the difference. Results for several values of B are plotted in Fig. 4 against the index n. The peak occurring in $\Delta\rho'_{n1}$ vs n is seen to shift towards smaller n for increasing B, or the scale of the reciprocal lattice. The value of n at the peak is approximately proportional to $g_1^{-1/2}$. Within the interval in B shown, the vortex lattice parameter varies between two and four times the penetration depth, approximately. We assume in the following analysis that the contribution to $\langle|u(\vec{g})|^2\rangle$ from overlap between vortices is small, and that changing B changes only the scale of reciprocal-lattice space. Although it is not considered possible to detect anisotropy, we expect it to have negligible

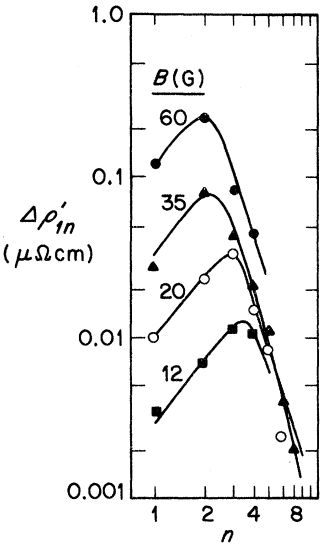

FIG. 4. Size of transition steps in rf resistivity vs subharmonic index number for several values of magnetic field. Solid curves are a smooth interpolation of theoretical points, at $n = 1, 2, 3, \ldots$ (not shown explicitly).

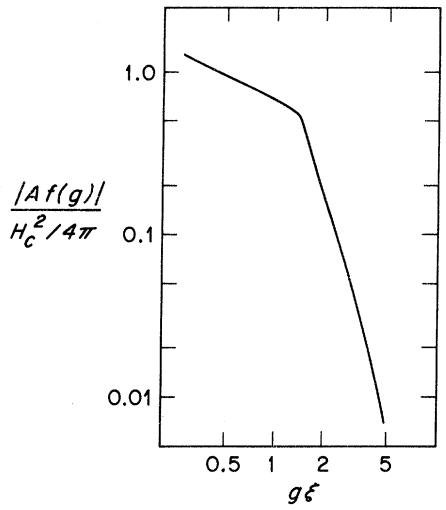

FIG. 5. Fourier transform of free-energy distribution, derived from measurements, vs reduced wave-vector magnitude. $B \ll H_{c2}$, $T \sim 0.8 T_c$.

effect for $B \ll H_{c2}$. Therefore, it is consistent to presume that $\langle |u(\vec{g})|^2 \rangle$ is a function of the magnitude $g = |\vec{g}|$.

A trial and error iterative procedure was used to unfold the sum in Eq. (7) to obtain the g dependence of the function $\langle |u(\vec{g})|^2 \rangle$. Certain properties of that sum are worth noting. In order that $\Delta\rho'_{n1}$ be an increasing function of n for small n (experimentally, approximately linear), $\langle |u(\vec{g})|^2 \rangle$ must behave as g^{-3} near $g = g_1$. The sharp peak observed in $\Delta\rho'_{n1}$ vs n requires a sharp knee in $\langle |u(\vec{g})|^2 \rangle$. Finally, the rapid decrease in $\Delta\rho'_{n1}$ for large n, as n^{-3} or faster, requires that $\langle |u(\vec{g})|^2 \rangle$ fall off as g^{-8} or faster. For each value of B, there is a set of values for $\langle |u(\vec{g})|^2 \rangle$ corresponding to a set of reciprocal-lattice vectors. By taking data at various values of the magnetic field, one varies the scale of g, establishing a form for $\langle |u(\vec{g})|^2 \rangle$ that is a continuous function of g. A set of calculated values for $\Delta\rho'_{n1}$, obtained from a best fit form for $\langle |u(\vec{g})|^2 \rangle$, are compared with the experimental values in Fig. 4 to illustrate the quality of the fit. To avoid confusing the calculated points with the experimental data, however, these results are represented by smooth curves which are drawn to connect points at $n = 1, 2, \ldots$. By fitting additional data taken at $B = 35$ G and at several other temperatures, the factorization indicated in Eq. (19) was verified. The g dependence of $|Af(\vec{g})|$ scales with $(H_{c2})^{1/2}$, or with ξ^{-1}, where ξ is the temperature-dependent coherence distance. These results are plotted in Fig. 5. It is evident from the symmetry that $Af(\vec{g})$ is positive definite. Also, from the temperature dependence, we find that the magnitude of $Af(\vec{g})$ contains a factor proportional to H_{c2}^2, over the interval $100 < H_{c2} < 300$ Oe, affirming the expected temperature dependence of the free-energy density.

Replacing the sum in Eq. (16) by an integral, the Fourier transform of $f(\vec{g})$ becomes a Hankel transform:

$$F(r) = \tfrac{1}{2}\pi \int_0^\infty J_0(gr) g A f(g)\, dg, \tag{21}$$

where $r = |\vec{r}|$ and J_0 is the Bessel function. Evaluated numerically, the free-energy density $F(r)$ is plotted in Fig. 6. The London theory approximation is used to establish the value of the one arbitrary constant by fitting the magnitude of $F(r)$ at large r to the prediction of that theory[21]:

$$F(r) \to \frac{1}{8\pi}\left(\frac{\varphi_0}{2\pi\lambda^2}\right)^2 \left[K_0^2\left(\frac{r}{\lambda}\right) + K_1^2\left(\frac{r}{\lambda}\right)\right], \tag{22}$$

where $\lambda = \kappa\xi$ and $\kappa = 3.0$ was used. K_0 and K_1 are modified Bessel functions of the second kind. The same value for this constant is found when all of the terms in the Ginzburg–Landau expression for the free energy are taken, and the calculated results, interpolated for $\kappa = 3$, of Neumann and Tewordt for the order parameter and magnetic field distributions are used.[14] Interestingly, the free-energy density along the vortex axis $F(0)$ turns out to be $1.5 H_c^2/4\pi$, which is significantly larger than the value predicted from Neumann and Tewordt's results, i.e., $0.6 H_c^2/4\pi$. More recently, Bardeen, Kümmel, Jacobs, and Tewordt have performed a microscopic calculation of the vortex structure.[15] Presuming that their calculation of the free energy due to states near the core has a spatial distribution scaling with the depression of the order parameter, we find that their theory predicts $F(0) = 3H_c^2/4\pi$. Although this result is intended to apply to pure superconductors at low temperatures, it provides a theoretical basis for expecting the bound and scattering states to enhance the core

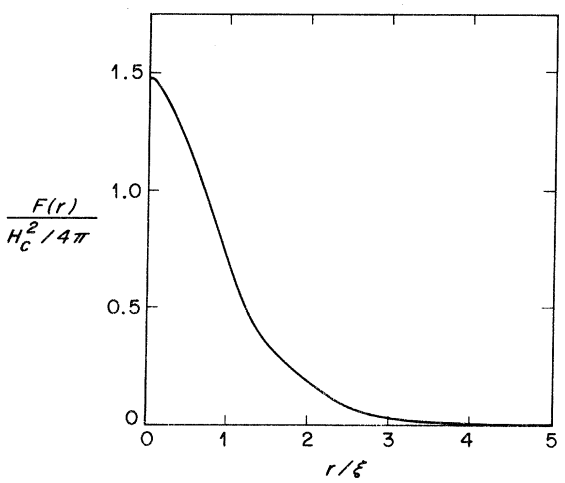

FIG. 6. Free-energy density vs reduced radial coordinate; the transform of the curve in Fig. 5.

free-energy density. Cleary has applied the approach of Bardeen *et al.* for temperatures near T_c, finding that the free energy is identical to the Ginzburg–Landau expression.[22] It would therefore be interesting indeed to apply the quantum interference technique to the pure type-II superconductors, niobium and vanadium, to which the abovementioned microscopic theories actually apply.

Results for the structure correlation function agree with the form given by Eq. (20), and the experimentally derived value for (σd) is 3.5×10^{-11} cm. Quoting Abeles measurements, i.e., $d=180$ Å, the coupling constant σ turns out to be 2×10^{-5}. In other words, the inhomogeneity among the grains is on the order of 0.4%.

Using somewhat larger applied rf currents than what was used in the course of obtaining the above results, it was found that transitions obeying Eq. (5) continued to be observable in magnetic fields as low as 0.5 Oe. This verification that the lattice parameter scales with $B^{-1/2}$ even at large values of intervortex spacing is taken to be a conclusive demonstration that the vortex-vortex interaction is repulsive at all separations.

For purposes of comparison, we mention recent neutron-diffraction measurements by Schelten, Ullmaier, and Schmatz of the magnetic field structure in an NbTa alloy (whose $\kappa=3.36$ is comparable to that of the aluminum film) and in pure niobium.[23] The NbTa results confirm calculations based upon Ginzburg–Landau theory and are consistent with our results on the aluminum film. In niobium, however, their evidence for an attractive interaction at large distances is quite clear: a maximum lattice parameter is found at low flux density. The attractive interaction is predicted by Dichtel's nonlocal theory.[24]

V. SHEAR ELASTIC MODULUS c_{66}

The shear modulus is computed from measurements of the width at half-maximum of the $n=1$ peak in plots of $d\rho'/dJ_{dc}$ vs E_{dc}, e.g., Fig. 3, using Eqs. (8)–(10) for $n=1$.

The above measurements and the width of the central half of the step in ρ' vs E_{dc} were found to be equal to within the uncertainty of the measurements. The chief source of error is the uncertainty in the location of a base line for the peaks in $d\rho'/dJ_{dc}$. It is largest at both ends of the magnetic field range covered and is estimated to be 20% or less. In order to use Eq. (10) to compute values of y_1, the pinning-potential correlation function derived in Sec. IV was used. It turns out that y_1 is small, lying in the interval $-0.2\le y_1\le0.2$ over the extent of the range of the data. Accordingly, z_1 is confined to the interval $0.9\le z_1\le1.1$ The following expression was then used to compute values of c_{66} from the measured widths:

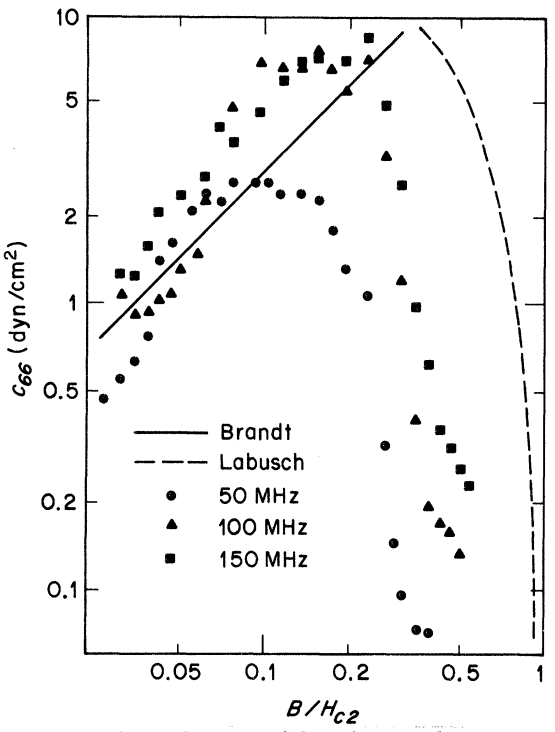

FIG. 7. Shear elastic modulus of vortex lattice measured at three frequencies and two theoretical curves vs reduced magnetic field. Dashed curve, Eq. (12); solid curve, Eq. (11). For theoretical results of Fetter *et al.* and of Matricon, refer to the text. $H_{c2}=260$ Oe.

$$\left(\frac{\delta E}{E}\right)_{11}=\frac{2\omega\eta Bz_1}{3g_1^2\varphi_0 c_{66}}. \tag{23}$$

The measured differential dc resistivity was used to obtain measured values for η, defined in the usual manner:

$$\eta=\frac{B\varphi_0}{c^2\rho_f}, \tag{24}$$

$$\rho_f=\left(\frac{dE_{dc}}{dJ_{dc}}\right)_{E_{dc}=E_{11}}. \tag{25}$$

Results for c_{66} are plotted in Fig. 7, for three values of the measuring frequency, against reduced magnetic field. Here, $H_{c2}=260$ Oe, and $T=1.18$ K. For comparison, theoretical curves derived from Brandt's[11] results at low field, Eq. (11), and Labusch's[19] result at high field, Eq. (12), are also shown. Agreement with theory at low magnetic field is quite good. The data also agree with the results of Fetter *et al.*[10] (not represented in Fig. 7) which correspond to a line 6% above the Brandt result. Matricon's result apparently contains a factor of ~6 error.[12] For very low magnetic fields $B\lesssim5$ G excitation of compressional lattice fluctuations is theoretically also important, since

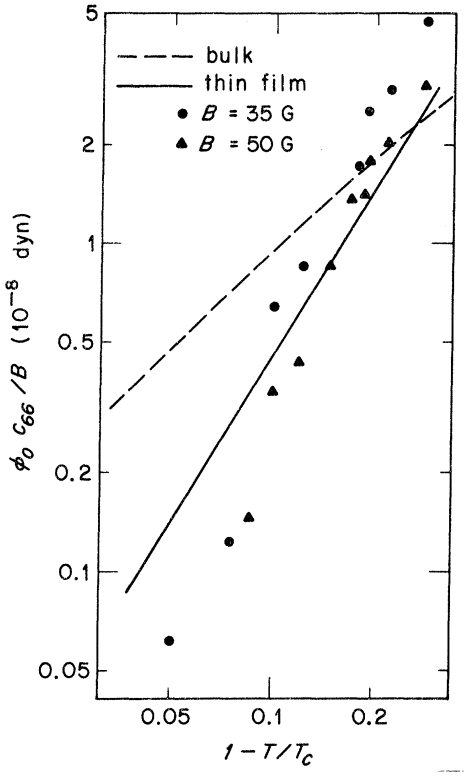

FIG. 8. Reduced shear modulus vs reduced temperature difference from T_c. Dashed curve is Eq. (11) for $\kappa = 3.0$. Solid curve is Eq. (11) for $\kappa = \kappa_{eff}$, as given by Eq. (26).

the compressional modulus vanishes as B^2 in the low-field limit.[11] Unfortunately, it is difficult to obtain data in this region that is good enough to check this out. In attempting to analyze data taken at $B \lesssim 10$ G one finds that both the widths of the transition peaks become large as B approaches zero and that their base lines become increasingly nonlevel.

Results for c_{66} at high magnetic field are, at first impression, at variance with the theory. Although according to Labusch's theory the shear modulus is expected to vanish at H_{c2}, we seem to have found a rather anomalous transition near $\frac{1}{2}H_{c2}$. Note also, that the value of the field at which this transition occurs increases with increasing measuring frequency.

It seems reasonable to attribute this apparent decrease in c_{66} to the onset of especially strong pinning forces at high magnetic field. This specimen displays the commonly observed "peak effect" in the dc pinning current at about the same field as the anomalous transition occurs. Should the pinning forces excite very large-amplitude shear deformations of the vortex lattice, large fluctuations induced in the vortex spacing and the angle of orientation of the lattice with respect to $\vec{e}_v$ would increase the observed width, indeed, washing out the interference structure altogether. The rms fractional fluctuation in vortex spacing, an estimate made from the Schmid theory, is approximately $(1/2\pi)(\delta x J_p/J)^{1/2}$. The conclusion here is that these data cannot be used as a test of the theory for the transition at H_{c2}.

A study of the temperature dependence of low-field data, which follows, does give a meaningful description of the transition at T_c. Temperature dependence of $\varphi_0 c_{66}/B$ is shown in Fig. 8. For taking these data, the magnetic field was kept fixed at either 35 or 50 G, and the measuring frequency at 150 MHz. It was discovered that the magnetic field value at which the peak effect washes out the transitions is an increasing fraction of H_{c2} as T approaches T_c. Therefore, even though B was kept fixed, the influence of the peak effect on the data presumably remains negligible over most of the temperature range covered. This opinion is supported by the fact that $\varphi_0 c_{66}/B$ is insensitive to B as it theoretically should be.

The dashed theoretical curve in Fig. 8 is computed from Brandt's theory.[11] That the data show a more rapid temperature dependence, the deviation becoming more pronounced close to T_c, is believed to be due to our approaching the thin-film limit: At $0.95T_c$ the (bulk) penetration depth would be seven times larger than the specimen thickness. If we ignore such questions as the validity of Eq. (11) in the thin-film limit and simply substitute an effective thin film κ_{eff} into that formula, we can get an approximate thin-film expression to compare with the experiment. For this purpose we use[25]

$$\kappa_{eff} = \frac{2}{(24)^{1/3}}\left(\frac{\lambda^2}{t\xi}\right)^{2/3} = 0.7\left(\frac{\kappa^2\xi}{t}\right)^{2/3}, \qquad (26)$$

where $\kappa = 3.0$ is the bulk value appropriate to the dirty aluminum, $T \sim T_c$. The result is drawn as a solid curve in Fig. 8, and appears as a much better fit to the data than the bulk limit (dashed curve).

The correct dispersion law for long-wavelength shear deformations has not been worked out in the thin-film limit, and is possibly not of the form $K_t q^2$ used in Eq. (1). As an illustration, if the law were $q^{3/2}$, for example, we find that Eq. (1) leads to transitions of a qualitatively different shape—instead of the sharp steps of Eq. (6), one gets $\rho' - \rho'_{n1} \propto (E_{dc} - E_{n1})^{1/3}$.

Another aluminum film had been studied, whose ratio of penetration depth to specimen thickness (at equal values of T/T_c) is five times larger than the specimen considered above, and that specimen had qualitatively similar transitions. Thus it seems that in the thin-film limit the only observable difference is a replacement of κ by κ_{eff}, and the fact that the vortex-vortex interactions are

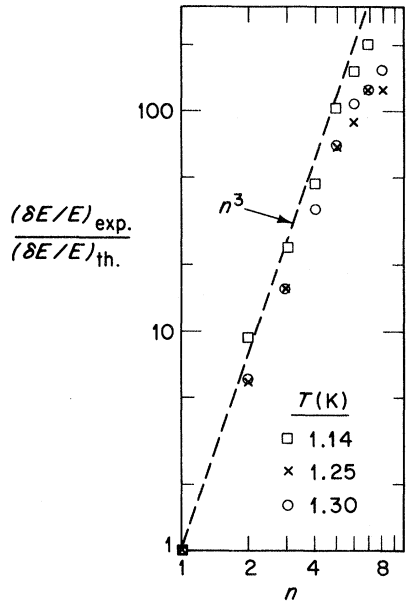

FIG. 9. Ratio of measured to theoretical transition widths vs subharmonic index for several temperatures at $B = 35$ G. Dashed n^3 line indicates trend of deviation.

functionally different is not apparent.

As a final point, we compare the widths of the complete sequence of steps, i.e., also $n > 1$, with those expected from the theory. We find that the widths are not proportional to n^{-3}, which is approximately the dependence predicted by Eqs. (8)–(10). In Fig. 9, a plot of the ratio of measured to theoretical widths (normalized to unity at $n = 1$) against n, we find an additional factor of n^3 which stands as an unexplained disagreement with this particular detail of the Schmid theory.

VI. SUMMARY

We have shown that measurements of quantum interference transitions can be used as a technique for studying vortex-lattice interactions and structure. The Schmid theory contains parameters such as c_{66} and $\langle |u(\vec{g})|^2 \rangle$ for which values are obtained from the experimental data. The results are in good agreement with applicable theories of vortex structure at low magnetic field, and support the basic correctness of the phenomenological model of vortex motion. For the granular aluminum film used here, we obtain a measure of the correlation function of pinning defects, the free-energy structure of a vortex, and the shear modulus for weak vortex-vortex interactions. Pinning defects are, as expected, of mean size much smaller than the size of the vortex (ξ or λ). There is more free-energy density in the vortex core than Ginzburg–Landau theory predicts, and it is possibly due to the presence of core states similar to those calculated by microscopic theory. The shear modulus agrees with low-field theory of weak vortex-vortex interactions in the bulk. However, near T_c, there is more rapid temperature dependence, suggesting thin-film limiting behavior.

ACKNOWLEDGMENT

The author acknowledges useful correspondence with Professor A. Schmid and appreciates receiving a copy of his preliminary report.

[1]A. T. Fiory, Phys. Rev. Lett. **27**, 501 (1971).
[2]A. Schmid, University of Dortmund, Preliminary Report (unpublished).
[3]Y. Simon and P. Thorel, Phys. Lett. A **35**, 450 (1971).
[4]T. R. Brown and J. G. King, Phys. Rev. Lett. **26**, 969 (1971).
[5]I. O. Kulik, Zh. Eksp. Teor. Fiz. **50**, 1617 (1966) [Sov. Phys.-JETP **23**, 1077 (1966)].
[6]C. Caroli and K. Maki, Phys. Rev. **164**, 591 (1967).
[7]B. B. Schwartz, Phys. Lett. **20**, 350 (1966).
[8]P. P. M. Meincke, Phys. Lett. A **29**, 208 (1969).
[9]P. W. Anderson and A. H. Dayem, Phys. Rev. Lett. **13**, 195 (1964); A. H. Dayem and J. J. Wiegand, Phys. Rev. **155**, 419 (1967).
[10]A. L. Fetter, P. C. Hohenberg, and P. Pincus, Phys. Rev. **147**, 140 (1966). Here c_{66} is denoted by L [Eq. (C6b)].
[11]E. H. Brandt, Phys. Status Solidi **35**, 1027 (1969); c_{66} is denoted by μ [Eq. (35b)].
[12]J. Matricon, Phys. Lett. **9**, 289 (1964); c_{66} is denoted by L.
[13]P. P. M. Meincke and W. A. Reed, Phys. Rev. **179**, 463 (1969).
[14]L. Neumann and L. Tewordt, Z. Phys. **189**, 55 (1966).
[15]J. Bardeen, R. Kümmel, A. E. Jacobs, and L. Tewordt, Phys. Rev. **187**, 556 (1969).
[16]K. Yamafuji and F. Irie, Phys. Lett. A **25**, 387 (1967).
[17]For a recent review, see W. W. Webb, J. Appl. Phys. **42**, 107 (1971).
[18]A. I. Larkin and Yu. N. Ovchinnikov, Zh. Eksp. Teor. Fiz. **61**, 1221 (1971) [Sov. Phys.-JETP **34**, 651 (1972)].
[19]R. Labusch, Phys. Status Solidi **19**, 715 (1967).
[20]B. Abeles, R. W. Cohen, and G. W. Cullen, Phys. Rev. Lett. **17**, 632 (1966). R. W. Cohen and B. Abeles, Phys. Rev. **168**, 444 (1968).
[21]For a review, see A. L. Fetter and P. C. Hohenberg, in *Superconductivity*, edited by R. D. Parks (Marcel Dekker, New York, 1969), Vol. 2, Chap. 14.
[22]R. M. Cleary, Phys. Rev. B **1**, 1039 (1970).
[23]J. Schelten, H. Ullmaier, and W. Schmatz, Phys. Status Solidi (b) **48**, 619 (1971).
[24]K. Dichtel, Phys. Lett. A **35**, 285 (1971).
[25]A. L. Fetter and P. C. Hohenberg, Phys. Rev. **159**, 330 (1967).